Full-Field Displacement Measurement within a Metal-as-Insulation HTS Pancake

Mohamad-Rajab Alharake, Philippe Fazilleau, Aurélien Godfrin, Olivier Hubert

Full-Field Displacement Measurement within a Metal-as-Insulation HTS Pancake

Mohamad-Rajab ALHarake
DACM
Université Paris-Saclay, CEA
Gif-Sur-Yvette, France
mohamad.alharake@cea.fr

Philippe Fazilleau
DACM
Université Paris-Saclay, CEA
Gif-Sur-Yvette, France
philippe.fazilleau@cea.fr

Aurélien Godfrin
DACM
Université Paris-Saclay, CEA
Gif-Sur-Yvette, France
aurelien.godfrin@cea.fr

Olivier Hubert
LMT
Université Paris-Saclay, ENS Paris-Saclay, CNRS
Gif-Sur-Yvette, France
olivier.hubert@ens-paris-saclay.fr

***Abstract*—In situ measurement of metal-as-insulation (MI) high temperature superconductor (HTS) pancake magnet deformation gives insight to its actual mechanical state. Measurement of hoop strain for inner / outer turn of MI pancake is possible locally using strain gauges. Hence, to avoid this local measurement limit, non-contact full-field displacement measurement is adopted. This technique is based on digital image correlation (DIC), which derives the displacement field in specified region of interest (ROI) by correlation between the deformed state image and the reference state image.**

In this article, we present a novel DIC experiment setup for displacement measurement of MI pancake in cryogenic cooling. It is used for cooling test of MI pancake made of co-wound copper beryllium - stainless steel 304 tapes after the setup is validated by a cooling test of stainless steel 304 disc due to its known properties, both tests using liquid nitrogen. Finally, experimental results are compared to numerical results obtained from an analytical formulation of the mechanical equilibrium using generalized plane strain assumption.

***Index Terms*—Digital Image Correlation, full-field displacement measurement, Metal-as-Insulation**

I. Introduction

In HTS superconducting magnets, especially at ultra high fields (UHF) [1], magnet sustains high Laplace force as it increases proportionally to square of magnetic field. However, due to slow quench propagation velocity in HTS tapes, no-insulation (NI) or metal-as-insulation (MI) HTS magnet configuration is adopted. They are adopted because of their protection against quench by current redistribution at quenched spot (hot spot) with next winding turn through contact between them. However, MI provides additional mechanical support when metal used is mechanically strong.

"Nougat" MI HTS insert magnet [2] is an example of UHF MI HTS magnet. It quenched at 32.5 T, with 14.5 T from HTS insert alone, without being damaged. Hence, full-field displacement measurement over MI HTS pancake will allow observation of magnet mechanical state while cooling and powering up. To circumvent strain gauge limitations [3] of local measurement, non-contact full field displacement is used with digital image correlation (DIC) [4]. DIC is used on large range of applications from room to elevated temperatures [4]. However, DIC application at cryogenic temperature have up to now been limited to [5]–[7] because of cryogenic difficulties (cooling, radiation heat load). Hence, a novel experiment setup is developed that will allow full field displacement measurement of MI HTS pancake in cryogenic cooling (from room to superconducting temperature). In order to verify the operating of the setup, a full stainless steel 304 (SS304) disc was tested by cooling as its properties are known. Then, a pancake made with copper beryllium and stainless steel tapes (MI CuBe2 / SS304) was tested to see MI pancake displacement by cooling contraction. Both samples (Table I, specifications) were tested in liquid nitrogen. The experimental results are compared with analytical ones derived from mechanical equilibrium using generalized plane assumption.

II. Experimental Setup

A. Setup Design

Several points are taken into account in setup design, mainly image acquisition and heat load while considering dimensions of the vertical cylindrical cryostat in which setup is inserted. This cryostat has liquid nitrogen and vacuum shielding.

Regarding image acquisition, a clear path between camera, light and the sample is provided using fused silica optical windows on cryostat flange. In addition, setup is used while having a cryogenic liquid bath inside bottom of cryostat which reaches below brass support level, so limiting heat load is required to avoid continuous evaporation of liquid bath. Cooling is done by conduction using tinned copper braids that are immersed in liquid bath and clamped onto brass support for sample cooling and G10 cooling support to maintain position. Aluminum shields are used as thermal grounding for all sensor wires while allowing clear image acquisition of sample. Considering image acquisition and cooling in the design (Fig. 1), a setup was manufactured.

TABLE I
SAMPLES

SS304 Disc	
Inner / Outer Radius	4 mm / 50 mm
Width	4 mm
MI CuBe2 / SS304 Pancake	
Brass 70/30 Mandrel Inner / Outer Radius	22 mm / 25 mm
Brass Width	6 mm
CuBe2 tape Thickness / Width	50 μm / 6 mm
SS304 tape Thickness / Width	50 μm / 6 mm
Number of Turns	50
Overbanding Thickness	0.35 mm
Pre-Tensioning	15.7 N

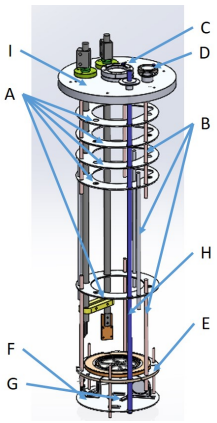

Fig. 1. Setup Design: A: aluminum heat shield, B: G10 support rod, C: camera window, D: light window, E: brass support, F: G10 cooling support, G: cooling braid copper clamp, H: cryogenic liquid input tube, I: cryostat flange

B. DIC Setup

A LabVIEW program was used to acquire and register the images into a data file. It was also used to monitor and synchronize the image acquisition with the temperature measurements of the sample, the brass support, and others parts of the setup. Camera is triggered with a trigger cable which is connected to a relay controlled by NI 9269 module using LabVIEW. Images are saved directly on the computer with EOS utility controlling camera and allowing live view inside cryostat.

Images are acquired using Canon EOS 5D Mark IV with Canon lens EF 70 - 200 mm f/4 IS USM being used at 200 mm focal length. Sample is illuminated by a constant white light from a LED pointer (Effilux-Sharp-FL-FF, 5W). With camera being at stand-off distance approximately 1300 mm from sample, camera is adjusted to have good quality images using ISO 800, aperture F8.0, shutter speed 1 / 400 s, and raw image quality (6720 x 4480 pixels). The setup is mounted outside cryostat at room temperature and adjusted (1 image every 30 s is acquired). Then, images are analyzed with Correli 3.0 [8] that is developed by LMT ENS Paris Saclay.

C. Experimental Procedure

Speckle pattern is applied on sample by spraying Boron Nitride white layer on it then fine spray of black matt paint

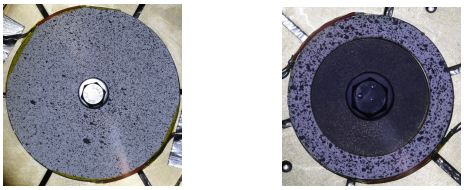

Fig. 2. (a) SS304 Disc; (b) MI CuBe2 / SS304 pancake

to have good contrast between black and white. Sample is centered on brass support disc. Then, pancake and setup are inserted inside cryostat (leak tight). To avoid ice formation inside cryostat, nitrogen atmosphere is created inside of it by flushing with nitrogen gas three times. The LabVIEW program, which is used for data and image acquisition, is started then cryostat is filled with liquid nitrogen till it reaches the level below the brass support. Images are acquired from room to cryogenic temperature (80 K).

III. Cooling Tests and Result Analysis

A. DIC Results

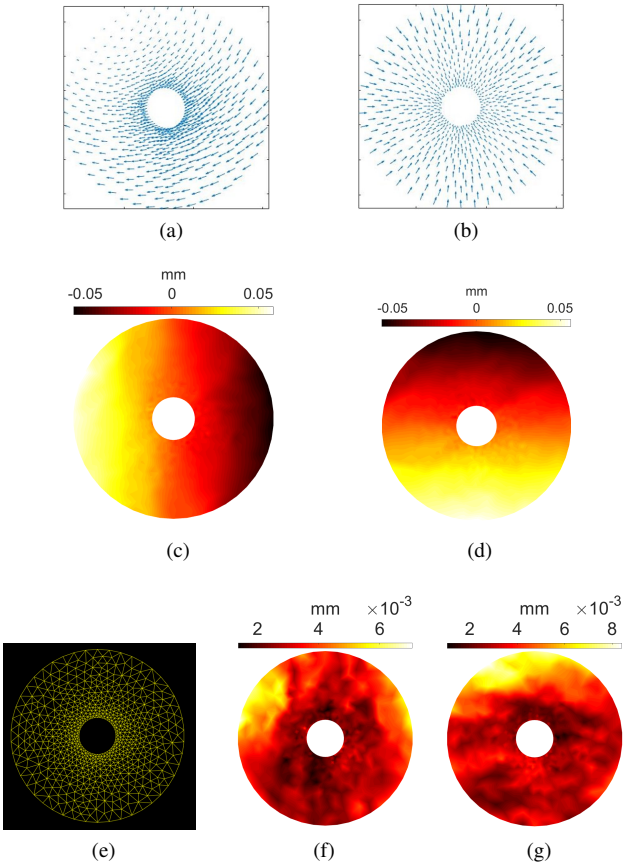

Fig. 3. SS304 disc: (a): Displacement Vectoring of DIC result without rigid body motion elimination (RBME); (b): Displacement Vectoring of DIC result with RBME; (c) / (d): Ux / Uy Field Displacement of DIC with RBME; (e): TRI3 mesh of Elsize 71 pixel of SS304 disc; (f): Error measurement of DIC Ux displacement; (g): Error measurement of DIC Uy displacement

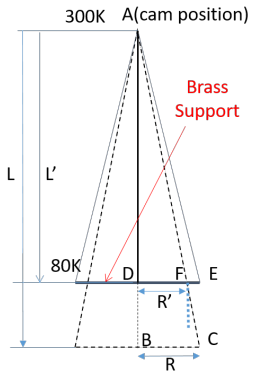

Fig. 4. Setup contraction sketch (dotted / solid: reference / contraction state)

SS304 disc (Fig. 2a) is cooled down from 296 K to 80 K. DIC is used (using reference and last deformed images) with a TRI3 finite element mesh of element size (Elsize) 71 pixel (Fig. 3e) (scale: 1 pixel: $\frac{1}{31}$ mm). It is noticed from Fig. 3a that results are not in accordance with thermal contraction phenomenon. Our explanation is that it is due to presence of rigid body motion (RBM) [9] (translation and / or rotation).

Hence, to get the DIC displacement, rigid body motion should be eliminated from measured displacement, which can be written as follows:

$$u^{'} = u + u^{RBM} \tag{1}$$

where $u^{'}$, u and u^{RBM} are, respectively, measured displacement, DIC displacement, and rigid body motion displacement. Rotation and translation of RBM are considered small in the experiment, expressed as in Eq. 2 (x_i, y_i are node coordinates, t_x, t_y are translations in x and y directions, θ is rotation angle).

$$u^{RBM} = (t_x e_x + t_y e_y + \theta(-y_i e_x + x_i e_y)) \tag{2}$$

Finding parameters of u^{RBM} is done using linear least squares fit (Eq. 3):

$$min\Sigma_i ||u(x_i) - (t_x e_x + t_y e_y + \theta(-y_i e_x + x_i e_y))||^2 \tag{3}$$

After removing RBM, post-processed DIC displacement measurement are that of thermal contraction which can be seen in Fig. 3b, 3c, and 3d. Results are in accordance with the thermal contraction direction (towards the center). Also, Fig. 3f and 3g show negligible error in DIC measurement of Ux and Uy. It is calculated as mean of standard deviation of DIC measurement of several images at same cryogenic temperature (80 K).

B. Comparison with Analytic Calculation

Total radial displacement is extracted as mean of displacement from 0 to 2 π at each radius (Eq. 4):

$$u_T(r_k) = \frac{1}{n}\sum_{1}^{n} u_{FT}(r_k)(\theta_i) \tag{4}$$

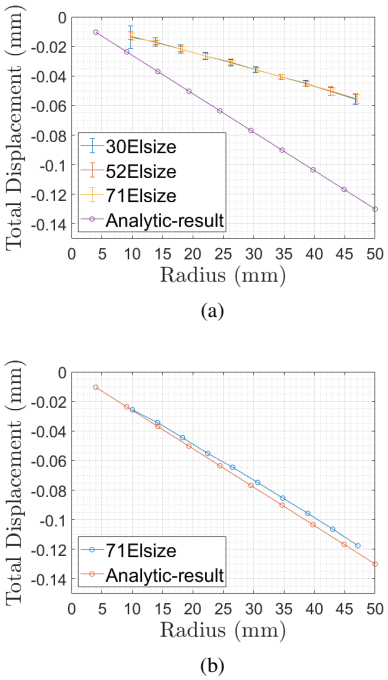

Fig. 5. Cooling test of SS304 Disc: (a): DIC displacement using different meshes and analytic displacement; (b): True displacement (DIC displacement after adding setup contraction effect)

where u_T and u_{FT} are respectively total radial displacement at specific radius and total radial displacement of mesh point from field displacement at same specific radius.

Total displacement is compared to analytic calculation using generalized plane strain assumption (see the Appendix) (Fig. 5a) showing significant difference between the two results with negligible difference in results between different meshes (Fig. 5a, error bar being standard deviation of u_{FT}). We explain this difference of displacement as result of total axial setup contraction that moves sample closer to camera. DIC is done using reference and deformed images. However, deformed image is taken after setup contraction, resulting in sample being slightly closer to camera than its initial position, enlarging it slightly. Hence, DIC displacement is sum of actual displacement of sample and magnification (apparent) displacement due to setup axial contraction. With sample being circular and uniform magnification, magnification effect is a constant positive radial strain to be derived (Eq. 6), and it is related to setup contraction (Fig. 4). Sample is assumed to remain in same shape when setup contracts.

The total setup contraction is α_T. This latter is calculated using the temperature measurements and the thermal contraction of G10 support rods, and it is expressed as follows:

$$\alpha_T = \int_{T1}^{T2} \alpha(T) dT \tag{5}$$

where T1 is greater than T2 and $\alpha(T)$ is thermal contraction coefficient of G10 rod [10]. It yields total contraction of α_T = -13.86 E-4 mm/mm. In addition, α_T can be expressed in another way as "$\alpha_T = \frac{L'-L}{L}$", where L and L' are distance

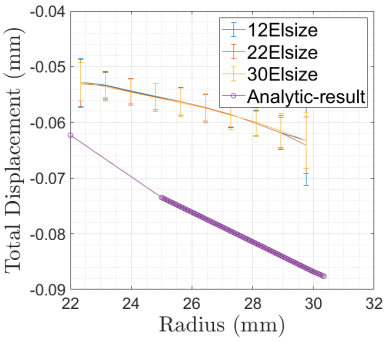

(a)

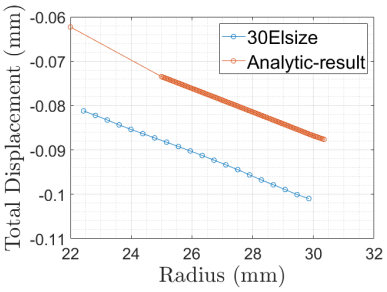

(b)

Fig. 6. Cooling of MI CuBe2 / SS304 pancake: (a): DIC displacement using different meshes and analytic displacement (290 K to 80 K); (b): DIC displacement after adding setup contraction effect

from flange to brass support before and after setup contraction respectively.

Sample remains in field of view of camera even after contraction, and from Fig. 4, it is seen that apparently a part is outside field of view. This part represents the magnification effect of setup contraction, and it can be expressed as apparent strain "$\epsilon_{rr} = \frac{R-R'}{R}$".

$$\epsilon_{rr} = \frac{R-R'}{R} = \frac{L-L'}{L'} = \frac{-\alpha_T}{1-\alpha_T} \approxeq \frac{-\alpha_T}{1} = -\alpha_T \quad (6)$$

Hence, actual contraction displacement of SS304 disc is expressed as follows:

$$u_r = u_{rDIC} - u_{rimage} = u_{rDIC} - r\epsilon_{rr} \quad (7)$$

where r, u_{rDIC} and u_{rimage} are respectively radius, DIC displacement without RBM and displacement caused by image magnification due to setup contraction.

In Fig. 5b difference between analytic and actual displacement is small, which is only due to total contraction that was calculated using temperature measurement from sensors placed on current leads and not G10 rods. Hence, with the correspondence of experimental and analytic results of SS304 disc cooling test, clear images for DIC calculation, and good conduction cooling (80 K), setup is validated.

After validation of setup, MI CuBe2 / SS304 pancake (Fig. 2b) is tested. It is cooled down from 290 K to 80 K. Mechanical regularization [11] is used in DIC calculation of MI pancake to minimize noises. It is used because speckle area is small and few pixels covering it (its width is $\approx$ 240 pixels, where as image is of size 6720 x 4480 pixels). Regularization length used in DIC is 24 pixels.

Total displacement of MI pancake is lower than that of analytic calculation without considering setup contraction (Fig. 6a) with negligible difference between different mesh results (Fig. 6a). However, when setup contraction correction (α_T = -12.9 E-4 mm/mm, it is temperature measurement dependent) is applied (Fig. 6b), the experimental results become higher than analytic by approximately 0.02 mm. This is probably due to thermal contraction of brass mandrel being higher than value used from reference [12], or setup contraction calculated not precise because of temperature sensors being on current leads and not G10 rods. Additional tests are needed to specify what is the cause of such results.

IV. Conclusion

A novel setup is designed that allows full field displacement measurement of MI pancakes. To acquire actual displacement, rigid body motion elimination and setup contraction effect are to be implemented. Moreover, proper speckle preparation and DIC setup calibration are important for good results [4] as image and speckle quality affect DIC results. In addition, temperature measurement of G10 support rods is necessary for proper calculation of setup contraction effect.

From SS304 disc liquid nitrogen cooling test, image acquisition and setup are validated. It showed that speckle used functioned at cryogenic temperature without an issue. Also, DIC yielded proper result despite non-vacuum cryogenic environment where convection can affect image quality. In addition, as shown from MI CuBe2 / SS304 test, more tests are required to pinpoint the reason for the difference between analytic and experimental results. After that, next step is to do same test with liquid helium to verify cryogenic helium handling, then energizing (current ramping) test of an MI HTS pancake with liquid helium.

Acknowledgment

The authors would like to thank Hugo Reymond and Jean-Christophe Gillard for setup manufacturing, Charles Maillert for his help with realizing the liquid nitrogen cooling test (cryogenic handling), and Prof. Francois Hild for his help regarding DIC questions.

Appendix
Generalized Plane Strain Cooling

$$u'' + \frac{u'}{r} - k^2\frac{u}{r} = -\frac{C_{rz}-C_{\theta z}}{C_{rr}}\epsilon_z^{tot} + \frac{C_{rr}-C_{\theta r}}{C_{rr}}\alpha_r + \frac{C_{\theta r}-C_{\theta\theta}}{C_{rr}}\alpha_\theta + \frac{C_{rz}-C_{\theta z}}{C_{rr}}\alpha_z \quad (8)$$

where u, r, C and k are respectively radial displacement, radius, orthotropic stiffness matrix (9) and k is anisotropy factor ($k^2 = \frac{C_{\theta\theta}}{C_{rr}}$).

$$S = \begin{bmatrix} C_{rr} & C_{\theta r} & C_{zr} \\ C_{r\theta} & C_{\theta\theta} & C_{z\theta} \\ C_{rz} & C_{\theta z} & C_{zz} \end{bmatrix} \quad (9)$$

REFERENCES

[1] R. Gupta et al., "Status of the 25 T 100 mm bore HTS solenoid for an axion dark matter search experiment", IEEE Trans. Appl. Supercond., vol. 29, no. 5, Aug. 2019.

[2] Philippe Fazilleau et al. "38 mm diameter cold bore metal-as-insulation HTS insert reached 32.5 T in a background magnetic field generated by resistive magnet". In: Cryogenics 106 (Mar. 2020)

[3] Y. Kim, et al., "Strain in YBCO double-pancake coil with stainless steel overband under external magnetic feld" IEEE Trans. Appl. Supercond., vol. 25, no. 3, Jun. 2014, Art. ID 4300504.

[4] International Digital Image Correlation Society, Jones, E.M.C. and Iadicola, M.A. (Eds.) (2018). A Good Practices Guide for Digital Image Correlation.

[5] H C Zhang et al 2017 IOP Conf. Ser.: Mater. Sci. Eng. 278 012083

[6] Wang X, Zhou Y, Guan M, Xin C. "A versatile facility for investigating field-dependent and mechanical properties of superconducting wires and tapes under cryogenic-electro-magnetic multifields". Rev Sci Instrum. 2018 Aug;89(8):085117.

[7] J. Pelegrin and W. O. S. Bailey and D. A. Crump "Application of DIC to extract full field thermo-mechanical data from an HTS coil" . IEEE Trans. Appl. Supercond., vol. 28, no. 4, Jun. 2018

[8] Leclerc H, Neggers J, Mathieu F, Hild F and Roux S 2015 Correli 3.0, IDDN. FR. 001.520008. 000. SP 2015.000.31500 Agence pour la Protection des Programmes Paris (France)

[9] A.S. Chernyatin, Yu.G. Matvienko, and P. Lopez-Crespo. "Mathematical and numerical correction of the DIC displacements for determination of stress field along crack front". In: Procedia Structural Integrity 2 (2016), pp. 2650-2658.

[10] "NIST, Index of Material Properties, Properties of solid materials from croygenic to room temperatures". Accessed: June 28,2021.[Online]. Available: https://trc.nist.gov/cryogenics/materials/materialproperties.htm

[11] Zvonimir Tomicevc, Francois Hild, and Stephane Roux. "Mechanics-aided digital image correlation". In: The Journal of Strain Analysis for Engineering Design 48.5 (June 2013), pp. 330-343.

[12] J. W. Ekin, "Experimental Techniques for Low Temperature Measurements", Oxford University Press, (2006)